remote sensing

MDPI

Article

Evaluation and Application of SMRT Model for L-Band Brightness Temperature Simulation in Arctic Sea Ice

Yanfei Fan [1], Lele Li [1,2,*], Haihua Chen [1,2] and Lei Guan [1,2]

[1] Faculty of Information Science and Engineering, College of Marine Technology, Ocean University of China, Qingdao 266100, China
[2] University Corporation for Polar Research (UCPR), Beijing 100875, China
* Correspondence: lilele@ouc.edu.cn

Abstract: Using L-band microwave radiative transfer theory to retrieve ice and snow parameters is one of the focuses of Arctic research. At present, due to limitations of frequency and substrates, few operational microwave radiative transfer models can be used to simulate L-band brightness temperature (TB) in Arctic sea ice. The snow microwave radiative transfer (SMRT) model, developed with the support of the European Space Agency in 2018, has been used to simulate high-frequency TB in polar regions and has obtained good results, but no studies have shown whether it can be used appropriately in the L-band. Therefore, in this study, we systematically evaluate the ability of the SMRT model to simulate L-band TB in the Arctic sea ice and snow environment, and we show that the results are significantly optimized by improving the simulation method. In this paper, we first consider the thermal insulation effect of snow by adding the thermodynamic equation, then use a reasonable salinity profile formula for multi-layer model simulation to solve the problem of excessive L-band penetration in the SMRT single-layer model, and finally add ice lead correction to resolve the large influence it has on the results. The improved SMRT model is evaluated using Operation IceBridge (OIB) data from 2012 to 2015 and compared with the snow-corrected classical L-band radiative transfer model for Arctic sea ice proposed in 2010 (KA2010). The results show that the SMRT model has better simulation results, and the correlation coefficient (R) between SMRT-simulated TB and Soil Moisture and Ocean Salinity (SMOS) satellite TB is 0.65, and the RMSE is 3.11 K. Finally, the SMRT model with the improved simulation method is applied to the whole Arctic from November 2014 to April 2015, and the simulated R is 0.63, and the RMSE is 5.22 K. The results show that the SMRT multi-layer model is feasible for simulating L-band TB in the Arctic sea ice and snow environment, which provides a basis for the retrieval of Arctic parameters.

Keywords: Arctic; snow microwave radiative transfer model; L-band TB; SMOS

Citation: Fan, Y.; Li, L.; Chen, H.; Guan, L. Evaluation and Application of SMRT Model for L-Band Brightness Temperature Simulation in Arctic Sea Ice. *Remote Sens.* **2023**, *15*, 3889. https://doi.org/10.3390/rs15153889

Academic Editors: Mohammed Shokr and Yufang Ye

Received: 22 June 2023
Revised: 30 July 2023
Accepted: 2 August 2023
Published: 5 August 2023

1. Introduction

The Arctic is an indicator and amplifier of global climate change and an important component of the global climate system. Sea ice and snow cover the Arctic surface all year round, and their high albedo and low thermal conductivity make them key factors of Arctic climate sensitivity and amplification [1]. Since it is difficult to obtain in situ observation data in the Arctic, remote sensing observation has become an important tool for research. Specifically, passive microwave remote sensing has high spatial and temporal resolution and is not affected by clouds, which makes it an important method for polar ice and snow observation. In order to retrieve parameters from satellite observations, we need to understand how the Arctic ice and snow parameters affect the brightness temperature (TB) measured by satellites. One of the important ways to understand this effect is to model the microwave radiative transfer process. Accurate modeling can explain the physical principles of the interactions between ice and snow, the atmospheric environment, and microwave signals, which is very important for the retrieval of Arctic ice and snow

parameters. In addition, model-based retrieval of Arctic parameters is an important means of supporting scientific research, resource utilization, and human activities in the Arctic. Through the retrieval of parameters such as sea ice extent and sea ice thickness, the Arctic ice situation can be effectively determined so as to avoid some natural disasters. For example, the reduction of sea ice exposes humans living near the Arctic to storm hazards [2], so it is necessary to strengthen the research of forward models and retrieval algorithms.

Several common, mature microwave radiative transfer models that can be used for passive microwave remote sensing of snow and ice are available internationally, including the Helsinki University of Technology (HUT) snow emission model [3], the microwave emission model of layered snowpacks (MEMLS) [4], and the dense media radiative transfer–multi-layer (DMRT-ML) model [5], among others. Royer et al. [6] compared the physical basis and microstructure settings for snow and ice of four commonly used snow and ice radiative transfer models (DMRT-ML, DMRT-QMS, MEMLS, HUT-nlayers) and showed that simulated TB at 11, 19, and 37 GHz was similar for each model when the microstructure parameters of snow were scaled. With research showing that snow cover has a significant effect on L-band microwave radiation, improved radiative transfer models for the L-band have been proposed in recent years. Based on the MEMLS and L-band microwave emission of the biosphere [7], Schwank et al. [8] proposed a radiative transport model of snow on a soil surface applicable to the L-band (LS-MEMLS), which is mainly applied to the study of frozen soil. Lemmetyinen et al. [9] improved the original HUT model, which contains one layer of snow, by proposing a multi-layer HUT model and validated it with in situ data in a glacial lake and proposed potential future applications for sea ice and snow. Leduc-Leballeur et al. [10] proposed the wave approach for low-frequency microwave emission in snow (WALOMIS) model, and experiments in Antarctica showed that the wave approach was more suitable than the radiative transfer model to simulate the L-band TB. Roy et al. [11] applied WALOMIS to snow in a prairie environment and compared it with the DMRT-ML and LS-MEMLS-1L models for L-band TB simulation, and the results showed that the root-mean-square errors of the three model simulations were similar at about 7.2~10.5 k.

However, due to frequency or substrate limitations, these operational models cannot be effectively applied to L-band TB simulations in the Arctic sea ice and snow environment. For example, the original MEMLS model is only applicable at 5–100 GHZ, while the HUT, DMRT-ML, and WALOMIS models are applicable to the L-band but cannot simulate the sea ice substrate. In 2013, Maaß et al. [12] improved the Burke model [13] by proposing a microwave radiative transfer model (called the M2013 model) consisting of a seawater layer, a single layer of sea ice, a single layer of snow, and an air layer, which achieved effective simulation of L-band TB in Arctic sea ice and snow. Zhou et al. [14] introduced sea ice temperature and salinity profiles based on M2013, refining the single-layer model into a multi-layer model and considering the effect of ice leads on TB, which greatly improved the accuracy of TB simulation. Miernecki et al. [15] added roughness analysis to the M2013 model to make the TB simulation results more accurate. Maaß et al. [16] improved the simple thermodynamic transport equation in the M2013 model using a more complex thermodynamic equation proposed by Tonboe et al. [17], which increased the TB interval of the model simulation and the sensitivity of the simulated TB to snow thickness. Richter et al. [18] added a layer of snow, considering only the insulation effect, to the classical sea ice microwave radiative transfer model (KA2010) proposed by Kaleschke et al. [19] and compared it with the M2013 model for L-band TB simulations, and the results showed that both models were able to capture the general variation of TB in the Arctic ice and snow. However, an operational microwave radiative transfer model for Arctic sea ice and snow was not available for any of these studies, which presented a challenge in the current study of the microwave radiative transfer model.

Picard et al. [20] proposed a next-generation microwave radiative transfer model, the snow microwave radiative transfer (SMRT) model, which can be applied to L-band TB simulation of Arctic sea ice and snow by selecting different ice and snow particle

microstructures and electromagnetic models through modular frameworks. The accuracy of this model depends on the parameter setting and structure selection, which has been extensively studied by scholars in recent years. Vargel et al. [21] compared simulated TB at 11, 19, 37, and 89 GHz by setting up different combinations of microstructure and electromagnetic models in SMRT to optimize TB simulations of Arctic and sub-Arctic snowpack, and the results showed that the improved Born approximation–exponential combination had the best results. Sandells et al. [22] reported the results of using the SMRT model to simulate TB, backscatter, and altimeter waveforms on snow surfaces with different substrates, demonstrating the model's ability to be used with active and passive observations. Based on in situ parameters of snow on frozen soil, Sandells et al. [23] used different snow microstructures in the SMRT model to compare TB simulations and noted that, due to the lack of stickiness, the simulation performance of the stickiness hard spheres microstructure model was poor, and the snow microstructure had an increasingly significant effect on the TB or backscatter simulation as the frequency increased. Picard et al. [24] described the calculation of electromagnetic properties (e.g., scattering and absorption coefficients) of each snow layer from microstructure parameters and applied it to the SMRT model. Picard et al. [25] used the SMRT model to study the sensitivity of Antarctic TB to the liquid water content of snow at five frequencies from 1.4 to 37 GHz, laying a foundation for future multi-frequency algorithms to detect snow and ice melting. Soriot et al. [26] used the SMRT model to simulate the TB of the common sea ice and snow environment in the Arctic in each band from 1.4 to 37 GHz to evaluate the ability of Copernicus Imaging Microwave Radiometer (CIMR) satellites to monitor ice and snow parameters, but TB simulation results of the L-band are still lacking. In summary, most of the current studies of the SMRT model are based on the land–substrate snow environment, and the accuracy of L-band TB simulations in the Arctic sea ice and snow has not yet been systematically verified. In order to use SMRT as an operational model for L-band TB simulation in the Arctic and apply it to the retrieval of Arctic parameters based on the L-band, it is necessary to systematically evaluate the model's ability to simulate the L-band TB in the Arctic sea ice and snow.

In this study, we explored the ability of the SMRT model to simulate the L-band TB of Arctic ice and snow and the feasibility of using it in Arctic-wide applications. Using Operation IceBridge (OIB) in situ data as the model input, we compared the simulation results of the SMRT and KA2010 models to evaluate the simulation capability of the SMRT model. Using satellite data as the model input, we examined the feasibility of using the SMRT model for large-scale application in the Arctic. In Section 2, the models and data used in this study are presented. In Section 3, we present the sensitivity analysis of the SMRT model, the data processing process, and the improvement of the simulation method for the SMRT model. In Section 4, we present the evaluation of the two models using OIB in situ data and the Arctic-wide application using satellite data. In Section 5, the causes of simulation bias are discussed. Section 6 summarizes the conclusions of this study.

2. Models and Data

2.1. Radiative Transfer Model

2.1.1. SMRT Model

Released in 2018, the SMRT model is a forward model developed with the support of the European Space Agency (ESA) for simulating microwave radiative transfer processes in snow. It integrates a number of ice and snow particle microstructure and electromagnetic models and can be used for snow TB simulations in various substrates, such as land, ice shelves, and sea ice. This model has been made open source for the community to use as a general framework for snow microwave radiative transfer models. The SMRT model can set the number of layers of ice and snow, and the interlayer relationship can be set to Fresnel plane or rough surface so as to take into account the reflectivity and transmittivity coefficients between snow and ice layers. The SMRT model can be used to build a single-layer or multi-layer model by inputting the physical parameters of each layer,

including snow thickness, temperature, density, radius, and stickiness, and ice thickness, temperature, salinity, density, radius, and stickiness. Figure 1 shows the model structure of SMRT, where h denotes the layer thickness, ρ and T denote the density and temperature of the corresponding medium, respectively, l denotes the number of layers, θ denotes the incident angle, I_0 denotes the atmospheric contribution, and I denotes the simulation result. The physical properties of snow and ice in each layer are related to the electromagnetic properties, mainly represented by permittivity (ε), absorption coefficient (Ka), extinction coefficient (Ke), and phase function (P).

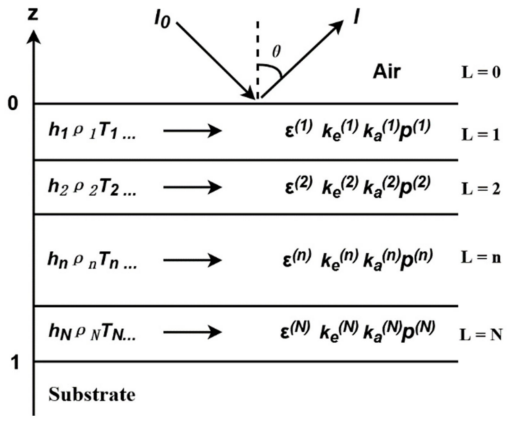

Figure 1. SMRT sea ice and snow model [20].

When using the SMRT model for simulation, the first step is to choose a suitable microstructure for ice and snow and a radiative transfer solution. The microstructure of ice and snow can be expressed as sticky hard spheres, exponential correlated particles, etc., and the particles are described by radius, stickiness, or correlation length. In this paper, we used the same model microstructure as the DMRT-ML model, sticky hard spheres, which can be applied to L-band microwave radiative transfer simulations.

The key component of the microwave radiative transfer model is the dielectric properties of sea ice, which is expressed as a calculation of effective permittivity. The permittivity value affects the penetration depth of the microwave signal within the sea ice and thus the saturation of TB on ice thickness. The dielectric properties of sea ice are mainly influenced by the brine volume fraction (Vb), which is calculated mainly by the ice and brine pocket contained in the ice. The SMRT model considers multi-year ice as a combination of ice, brine pocket, and air bubbles and uses the Polder–Van Santen formula [27] to calculate the permittivity of sea ice.

2.1.2. KA2010 Model

For comparison with the SMRT simulation results, we chose the radiative transfer model of Kaleschke et al. [19] to simulate TB at 1.4 GHz in Arctic sea ice and snow. KA2010 is a simple dielectric model consisting of only one layer of seawater, one layer of sea ice, and one layer of air and has been successfully applied to sea ice thickness retrieval [28]. Richter et al. [18] added a layer of snow, considering only thermal insulation, to the KA2010 sea ice model and compared it with the M2013 model for L-band TB simulation in the Arctic. Since the M2013 model is not open source, this paper refers to Richter et al. [18], adding a layer of snow to KA2010 and comparing with the simulation results of SMRT.

Different from the SMRT model, in the KA2010 and M2013 models and their improved versions, the permittivity of sea ice is calculated by an empirical formula. According to the experiments of Vant et al. [29], the permittivity of sea ice can be expressed as an equation of Vb, while Vb is expressed as a function of sea ice and brine pocket density and salinity [30]. The density and salinity of brine pocket can be approximated as a function of sea ice temperature [30].

2.2. Data

According to previous studies, ice and snow parameters such as snow thickness and sea ice type, concentration, thickness, temperature, and salinity have a great influence on TB, and these parameters should be as close to the real Arctic conditions as possible to make the simulation more accurate. In order to evaluate the simulation capability of the SMRT model and apply it to the whole Arctic, in situ data and satellite data products with corresponding parameters were used as the input of the model, and the satellite TB data were compared with the simulation results.

2.2.1. Model Input Data

When evaluating the model, we used in situ data. Operation IceBridge (OIB), an 11-year airborne mission over Earth's polar ice conducted by the National Aeronautics and Space Administration (NASA) from 2009 to 2019, flew at a low altitude of 450 m to provide in situ data of sea ice thickness, snow depth, freeboard, and surface temperature at 40 m resolution. In this study, the IDCSI4 version from 2012 to 2013 and the quick-look version from 2014 to 2015 were used, and the flight path of OIB campaigns during this period is shown in Figure 2.

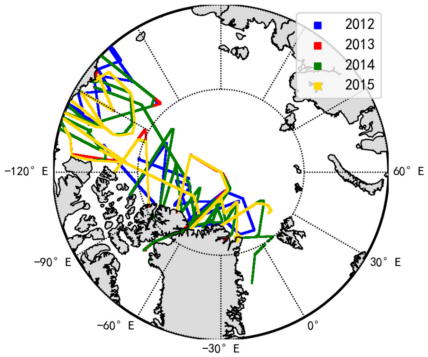

Figure 2. Flight path of OIB campaigns during 2012–2015.

When using satellite data as model input for Arctic-wide applications, multiple satellite products are required to provide the corresponding ice and snow parameter data. For ice and snow thickness, we used the merged SMOS–CryoSat Sea Ice Thickness Level 4 product and the AMSR-E/AMSR2 Unified Level 3 snow thickness product. SMOS–CryoSat L4 provides weekly averages with a spatial resolution of 25 km. Through the merging of the two satellite retrieval methods, the product uncertainty is optimized to about 0 to 1 m [31]. The AMSR-E/2 Unified Level 3 snow thickness product is obtained through an empirical relationship between the TB of Advanced Microwave Scanning Radiometer for EOS (AMSR-E) or Advanced Microwave Scanning Radiometer 2 (AMSR-2) satellites and the measured snow thickness; it provides daily averages with a spatial resolution of 25 km from January to May, November, and December every year. The uncertainty of snow thickness on first-year ice (FYI) is about 0.1–6 cm and on multi-year ice (MYI) is about 3.4–9.4 cm [32]. It should be noted that, due to algorithm limitations, this product only includes snow thickness on MYI in March and April [32].

For the surface temperature data, we used the MOD29E1D ice surface temperature (IST) product [33] from the Moderate Resolution Imaging Spectroradiometer (MODIS) satellite and ERA5 skin temperature data (SKT). MOD29E1D provides daily averages with a spatial resolution of 4 km which are obtained by re-projecting the 1 km resolution data of the MOD29P1D IST onto a 4 km resolution grid. However, MOD29E1D IST lacks a large amount of data in some months, so we used ERA5 SKT data to supplement it. The ERA5 reanalysis data comprise a global atmospheric reanalysis dataset provided by the European Centre for Medium-Range Weather Forecasts (ECMWF), covering a time range from 1950 to the present with a spatial resolution of 25 km and a temporal resolution of 1 h. In the

Arctic sea ice region, ERA5 SKT is calculated by assuming a constant ice thickness of 1.5 m, without taking into account the heat transfer of snow.

For sea ice salinity, the Multidisciplinary Drifting Observatory for the Study of Arctic Climate (MOSAiC) expedition provided sea ice temperature and salinity data for FYI and second-year ice (SYI) ranging from the early growth period in October 2019 to the warming period in May 2020. MOSAiC collected ice cores at different depths of sea ice to calculate the salinity at those depths and obtained an in situ salinity profile.

For sea ice type and concentration, we used global sea ice type and concentration data from the Ocean and Sea Ice Satellite Application Facility (OSI-SAF), which are daily average data with a spatial resolution of 10 km.

2.2.2. Auxiliary Data

Sea ice leads are long, narrow cracks formed by the movement of sea ice which can be water or refrozen thin ice and have an effect on the TB received by the satellite. In order to consider the effects of ice leads, we used the sea ice leads dataset provided by Willmes et al. [34]. The dataset is derived from MODIS thermal infrared imagery, which are daily average data with a spatial resolution of 1 km, and it is labeled with sea ice conditions: 0 for land, 1 for clouds, 2 for sea ice, 3 for artifact, and 4 for ice leads. The uncertainty is due to the limitation of thermal infrared, and the dataset cannot accurately judge the surface type in cloudy areas.

The Soil Moisture and Ocean Salinity (SMOS) satellite observes L-band microwave radiative emission from the Earth's surface at a frequency of 1.4 GHz. In order to test the accuracy of the model simulation result, we compared the L3B SMOS satellite TB data from the University of Hamburg [35] with simulated TB. The L3B TB dataset provides daily average brightness intensity (average TB of horizontal and vertical polarization) data at 12.5 km spatial resolution, which is the mean TB between 0° and 40° incidence angles. It is important to note that the physical resolution of SMOS observations is about 40 km.

2.2.3. Evaluation Metrics

In this paper, some evaluation metrics based on statistics were used to illustrate the accuracy of the model simulation results [36], including root-mean-square error (RMSE), correlation coefficient (R), and mean bias.

RMSE is a common statistic used to evaluate the simulation capability of a model. It reflects the magnitude of the bias by calculating the square root of the bias between the simulation results and the observed value. The smaller the RMSE, the better the simulation capability of the model. It is defined as:

$$\mathrm{RMSE} = \sqrt{\frac{1}{n}\sum_{i=1}^{n}(x_i - y_i)^2} \tag{1}$$

R is a statistic that reflects the degree of linear correlation between two variables. The most commonly used Pearson correlation coefficient is calculated as follows:

$$\mathrm{R} = \frac{\sum_{i=1}^{n}(x_i - \overline{x})(y_i - \overline{y})}{\sqrt{\sum_{i=1}^{n}(x_i - \overline{x})^2 \sum_{i=1}^{n}(y_i - \overline{y})^2}} \tag{2}$$

Mean bias directly reflects the overall deviation of the model simulation results by calculating the average error of the simulation results and the observed value, which is defined as follows:

$$\mathrm{E_{bias}} = \frac{\sum_{i=1}^{n}(x_i - y_i)}{n} \tag{3}$$

In Formulas (1)–(3), x and y respectively represent the two datasets used for comparison, and n represents the number of samples.

3. Methods

In addition to ice and snow thickness, surface temperature, and sea ice salinity, other parameters describing the microstructure of ice and snow are also required for the input data of the SMRT model, such as the radius, stickiness, and density of ice and snow. These parameters are difficult to obtain, but they have little effect on simulated TB, and previous studies usually used constant settings. The influence of each input parameter of the SMRT model on the simulated TB was obtained through sensitivity analysis so as to set the constant of parameters that are not sensitive to TB and conduct data preprocessing for the sensitive parameters. According to previous studies on snow and ice microwave models, the sensitivity results of the SMRT model, and the simulation results using OIB in situ data as input, the simulation method improves some disadvantages in the model. The improvement is mainly in three aspects. First, the thermodynamic equation of snow and ice was added, thus their thermal insulation effect was considered in the simulation. Second, the effects of the SMRT single-layer and multi-layer models and the corresponding salinity formulas on the simulation results were compared. Third, the simulation bias caused by ice leads was corrected by an empirical equation. Finally, the evaluated model was applied to the whole Arctic region using satellite data as input.

3.1. Sensitivity Analysis

In this paper, the sensitivity of the SMRT model was studied to obtain the sensitivity of simulated TB to each input parameter in order to determine whether the input parameters can be set as constants. We referred to Soriot et al.'s [26] parameter settings for FYI, MYI, and snow as the default input and conducted sensitivity studies on these parameters in SMRT's single-layer model (one layer of ice and one layer of snow) within a certain range. The default values and variation ranges [37,38] of parameters in the sensitivity study are shown in Table 1.

Table 1. Default values and variation ranges for sensitivity studies.

Type		Parameters	Defaults	Sensitivity Range
Sea ice	MYI	Ice thickness (m)	3	2~5
		Surface temperature (°C)	−30	−40~−25
		Ice salinity (PSU)	3.5	1~5
		Ice density (kg/m^3)	850	720~910
		Ice optical radius (mm)	0.1	0.05~0.3
		Ice stickiness	0.2	0.1~0.3
	FYI	Ice thickness (m)	1	0.5~2
		Surface temperature (°C)	−30	−40~−25
		Ice salinity (PSU)	10	5~12
		Ice density (kg/m^3)	910	840~910
		Ice optical radius (mm)	0.1	0.05~0.3
		Ice stickiness	0.2	0.1~0.3
Snow		Snow thickness (cm)	15	0~50
		Snow density (kg/m^3)	350	260~350
		Snow optical radius (mm)	0.16	0.05~0.3
		Snow stickiness	0.18	0.1~0.3

The sensitivity results are shown in Figure 3. It can be seen that the main factors affecting the simulated L-band TB are sea ice thickness, snow thickness, sea ice salinity, and surface temperature. The other parameters have less influence, so we set them as constants. The constant values refer to Soriot et al. [26], with snow optical radius set to 0.16 mm, snow stickiness to 0.18, snow density to 350 kg/m^3, sea ice optical radius to 0.1 mm, sea ice stickiness to 0.2, FYI density to 910 kg/m^3, and MYI density to 850 kg/m^3. The optical radius refers to the particle size of the scattering sphere in the microstructure of ice and snow.

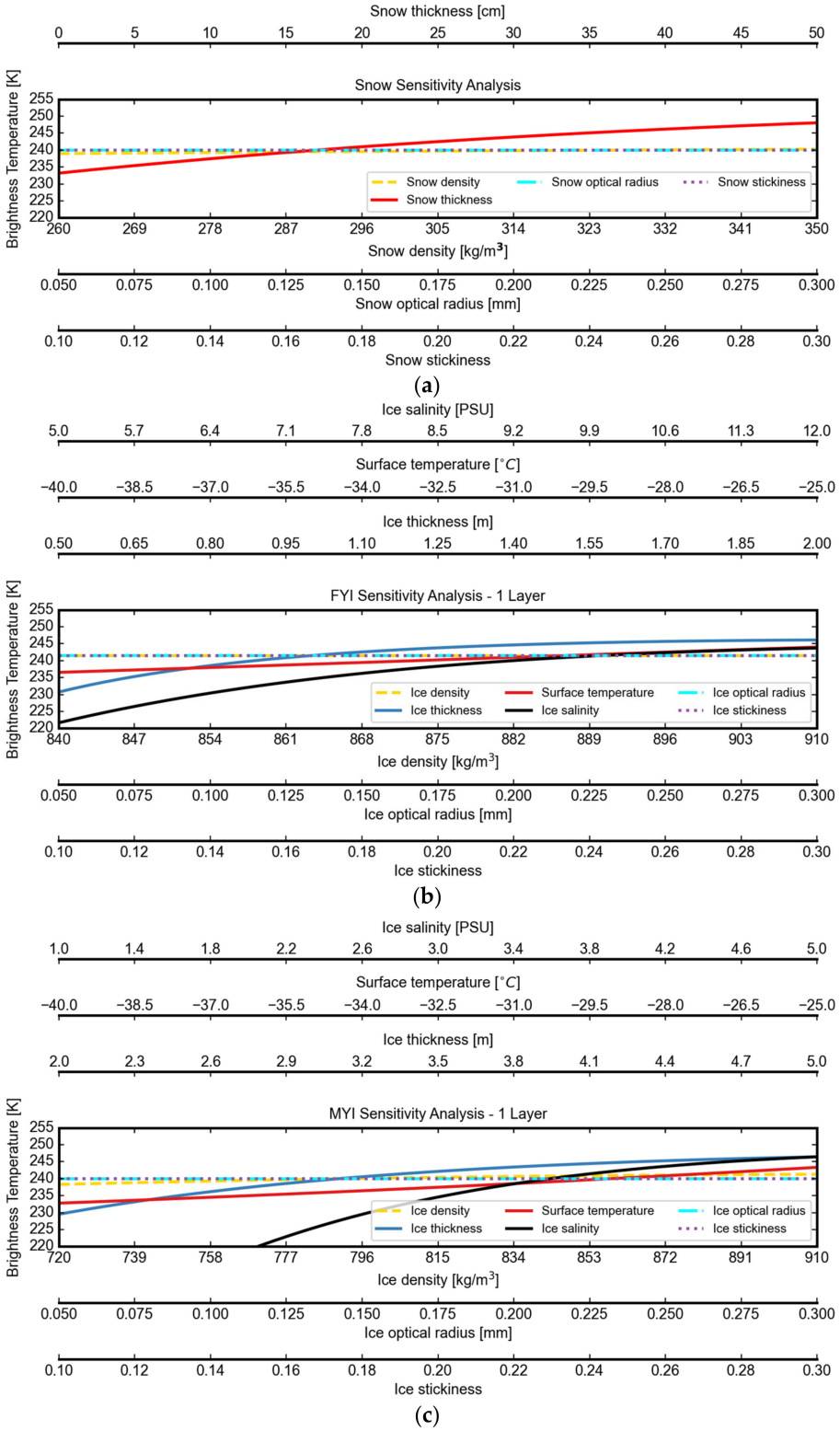

Figure 3. Sensitivity analysis of SMRT single-layer model. (**a**) Sensitivity analysis of snow parameters. (**b**) Sensitivity analysis of FYI parameters. (**c**) Sensitivity analysis of MYI parameters.

We compared the sensitivity of the SMRT single-layer model with the M2013 model. Taking MYI as an example for surface temperature and snow thickness, the performance of the SMRT model was relatively consistent with that of the M2013 model [12]. With MYI surface temperature ranging from −36 to −31 °C, the TB of M2013 changed by about 1.5 K, while that of SMRT changed by about 2 K. With snow thickness ranging from 0 to 40 cm, the

TB of M2013 changed by about 6 K and that of SMRT by about 10 K. The difference between the two models was mainly due to the difference in the default settings of other parameters. For sea ice thickness, the sensitivity of TB is mainly reflected in the penetration depth of ice thickness. That is, when the ice thickness increases to a certain amount, TB no longer changes due to the limited penetration capacity of the L-band. The microwave penetration depth is mainly related to sea ice salinity, which decreases with increased salinity. Here, the sensitivity of the two models to sea ice thickness was obviously different. For MYI, the penetration depth of the L-band in M2013 was about 2.5 m, while the SMRT single-layer model still had an excessive penetration depth of about 3.5 m at higher default sea ice salinity. Similarly, for FYI, SMRT exhibited an excessive penetration depth of about 1 m, while studies have shown that the L-band penetration depth for FYI is about 0.5 m [39]. In addition, for sea ice salinity, the simulated L-band TB of the SMRT single-layer model showed too much sensitivity. These phenomena indicate that the SMRT single-layer model is not capable of simulating L-band TB in the Arctic ice and snow environment.

3.2. Data Preprocessing

In the model evaluation stage, we used the in situ data of OIB from 2012 to 2015 for the sea ice thickness, snow depth, and surface temperature inputs of the SMRT model. Considering that the OIB provides in situ data with a spatial resolution of 40 m, and the physical resolution of SMOS satellite TB is about 40 km, we projected all the daily OIB points into 40 km grids to obtain gridded OIB data. In order to reduce data errors, only the grids with more than 200 OIB statistical points were taken, and data exceeding the mean by 3 standard deviations in each grid were removed during grid projection averaging.

In the whole Arctic application stage, for the input of SMRT model, we used the sea ice thickness data of SMOS-CryoSat, snow thickness data of AMSR-E/2, and surface temperature data of MOD29E1D and ERA5. Due to the presence of liquid water in snow caused by the melting of Arctic ice and snow in summer, the microwave signal was almost impenetrable, so we only simulated dry snow in winter and selected the time range from November 2014 to April 2015. From November 2014 to March 2015, days 1, 5, 10, 15, 20, 25, and 30 (28 in February) were selected to represent the corresponding month, and in April 2015, due to the lack of sea ice thickness data, only days 1 to 9 were selected to represent the entire month. These satellite data were projected into a 25 km grid, grids with sea ice concentration greater than 95% were selected, and data exceeding the mean value by 3 standard deviations in each grid were removed during grid projection averaging.

Two datasets, MOD29E1D and ERA5, were used for surface temperature, because MOD29E1D products lack a large amount of data in some months (Figure 4) and need to be supplemented by other surface temperature data, which, in this paper, were ERA5 SKT data. Since the MOD29E1D product is the result of daytime averages, in addition to the effect of cloud cover, some regions have a large deficiency due to lack of nighttime data.

Since ERA5 SKT data are obtained by model calculation under the assumption of no snow and constant sea ice thickness of 1.5 m, this simplification can produce large errors, especially when the snow thickness is large or the difference between the actual ice thickness and 1.5 m is large [40]; thus, ERA5 SKT needs to be corrected to reduce data errors. We used the MOD29E1D IST of the selected dates from November 2014 to April 2015 to fit and correct the ERA5 SKT so that the corrected ERA5 SKT could be used to fill the surface temperature data in the MOD29E1D vacant area. Data with a temperature lower than -1.8 °C were selected, and the comparison between ERA5 SKT before and after correction and MOD29E1D IST is shown in Figure 5.

In order to determine whether the relationship between MOD29E1D IST and ERA5 SKT was stable in different months of the year, we fitted the correlation to each month from November 2014 to April 2015, as shown in Table 2. For January to April, when the sea ice state was stable, the slope (a) varied between 0.65 and 0.71, and the intercept (b) varied between -3.4 and -2.1 °C. The fitting coefficients of the two were relatively stable in winter.

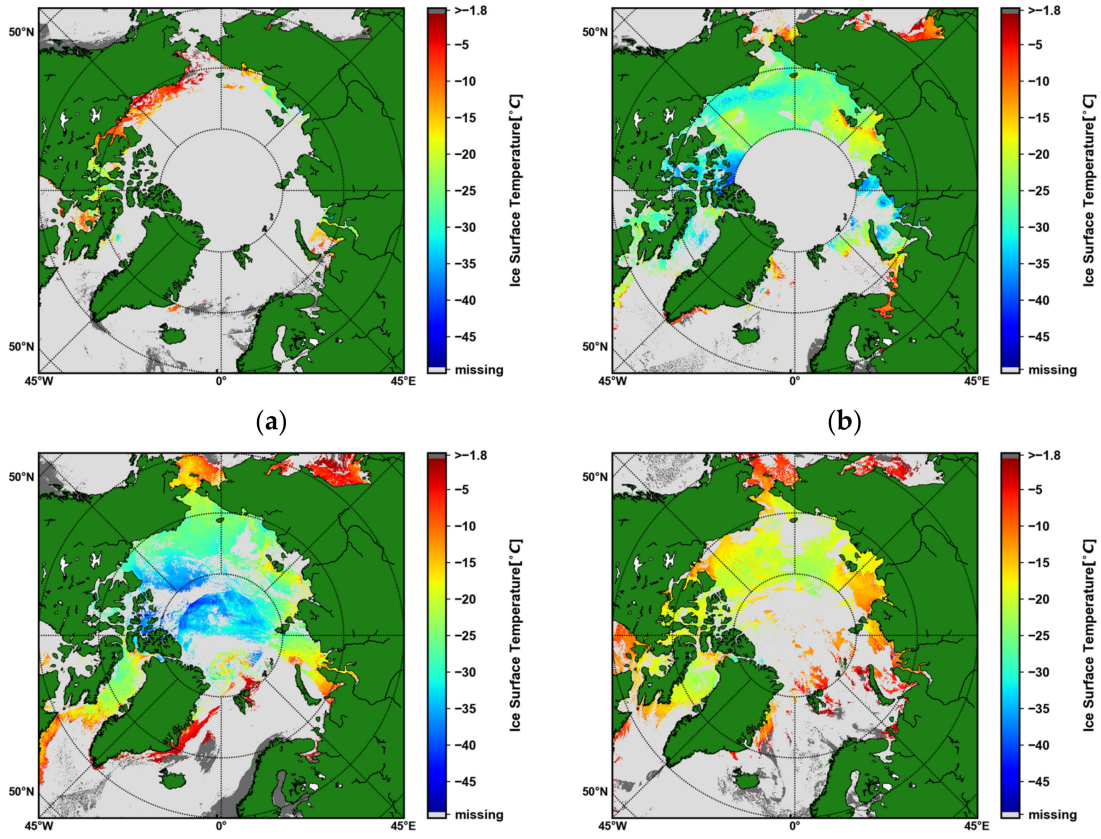

Figure 4. Absence condition of MOD29E1D IST from November 2014 to April 2015, taking the middle of each month for examples [33]. (**a**) November 2014–January 2015, taking 15 November 2014 for example. (**b**) 15 February 2015. (**c**) 15 March 2015. (**d**) 15 April 2015. Color bar displays the value of MOD29E1D IST less than −1.8 °C. In the background map, green is the continent, light gray is the missing data, and dark gray is the area where the IST is greater than −1.8 °C, which is regarded as invalid in this paper.

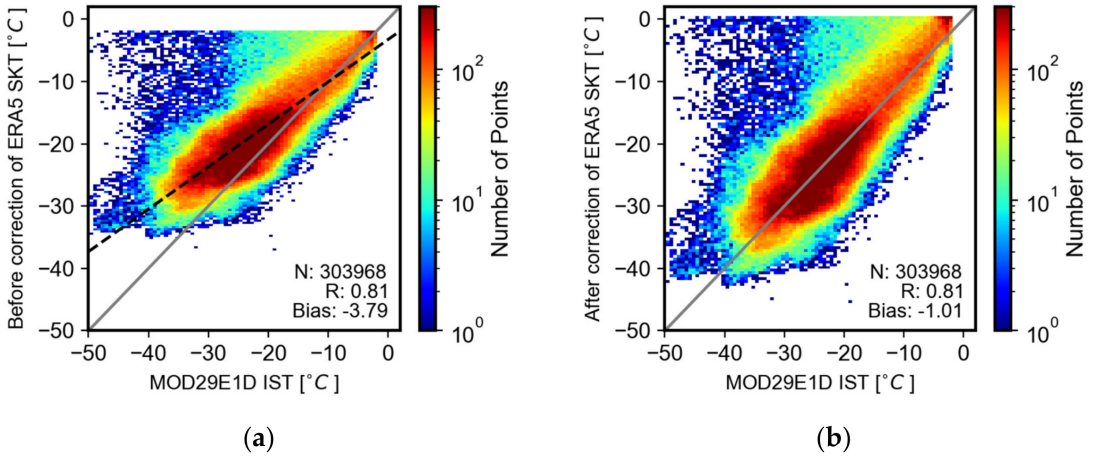

Figure 5. Correlation between MOD29E1D IST and ERA5 SKT for the selected dates from November 2014 to April 2015. (**a**) Before correction of ERA5 SKT. (**b**) After correction of ERA5 SKT. The gray lines are 1:1 lines, and the black dashed line is the least squares fit line.

Table 2. Fit coefficients and quantities of MOD29E1D IST and ERA5 SKT.

Date	N	a	b
November 2014	20,790	0.3868	−5.245
December 2014	8590	0.5320	−3.687
January 2015	17,678	0.7188	−2.135
February 2015	41,826	0.7117	−3.211
March 2015	79,426	0.6598	−3.421
April 2015	138,583	0.7116	−3.372
November 2014~April 2015	303,968	0.6806	−3.268

Finally, for the convenience of later calculations, Willmes's ice leads dataset was also projected onto a 25 km (or 40 km for the OIB experiment) grid. In addition, the labeled data within a grid were averaged to the proportion of ice leads.

3.3. Improvement of Simulation Method

3.3.1. Thermodynamic Equations

When snow covers the sea ice, it has a thermal insulation effect, that is, the snow/ice interface temperature ($T_{snow/ice}$) is greater than the surface temperature (T_{surf}). Since the simulation in this study includes a snow layer, we assumed that the snow temperature was the T_{surf}, and the ice temperature was the $T_{snow/ice}$. In addition, when using the multi-layer model, there is a temperature gradient inside the sea ice, which can be described as a linear change in temperature with depth based on the thermal conductivity of sea ice (k_{ice}), with $T_{snow/ice}$ at the top and sea water temperature (T_{water}) at the bottom, as shown in Figure 6.

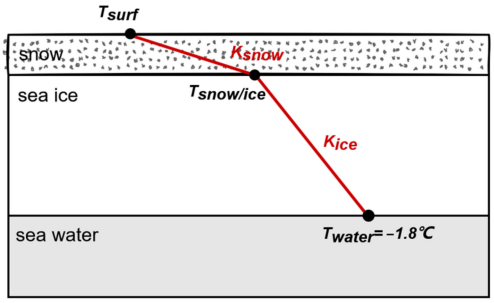

Figure 6. Thermodynamic temperature profile in the ice and snow.

For snow thermal conductivity, we used a constant value k_{snow} = 0.31 $Wm^{-1}k^{-1}$, and, for ice thermal conductivity, we used Formula (4) to set the value [41,42].

$$k_{ice} = 2.034\ \mathrm{Wm^{-1}k^{-1}} + 0.13\ \mathrm{Wkg^{-1}m^{-2}}\frac{S_{ice}}{T_{ice} - 273.15} \quad (4)$$

where k_{ice} is the ice thermal conductivity, S_{ice} is the bulk salinity of sea ice in PSU, and T_{ice} is the bulk ice temperature in K. In the original SMRT model, snow and ice are modeled separately, with sea ice temperature and snow thickness as external inputs to the model, and no relationship between the two is established. We used the thermodynamic equation to describe sea ice temperature as a function of T_{surf} and snow thickness in order to reflect the thermal insulation effect of snow on ice in the SMRT model. By combining the SMRT model and the thermodynamic equation, we could simulate the physical transmission process of L-band microwave signals in the Arctic sea ice and snow environment.

3.3.2. Sea Ice Salinity

Among the main factors influencing simulated TB, there are satellite, reanalysis, and in situ data for snow thickness, sea ice thickness, and surface temperature, while there are no available data for sea ice salinity. Ice salinity directly affects the dielectric properties of

sea ice and has a great impact on the simulation process. Setting it as a constant may cause a large error, so previous studies often used empirical formulas. Since the SMRT model can set the sea ice as a single-layer or multi-layer model, in this paper, we compared the single-layer and multi-layer models and used the corresponding sea ice salinity formulas (bulk salinity for single-layer model and salinity profile for multi-layer model) to select the appropriate SMRT model and salinity formulas.

For sea ice bulk salinity in the single-layer model, the empirical relationship of bulk salinity with ice thickness described by Cox and Week et al. [43] shows that bulk salinity decreases with increased ice thickness in winter, and the bulk salinity of ice at any thickness is about 2 PSU in summer. Vancoppenolle et al. [44] used a salinity model to observe the variation of sea ice salinity and noted that bulk salinity is seasonally dependent in addition to being affected by sea ice thickness. The seasonal variation of bulk salinity with ice thickness is shown in Figure 7. It can be seen that the seasonal equations derived from Vancoppenolle's salinity model are in good agreement with the Cox winter equation in March and December during the winter months.

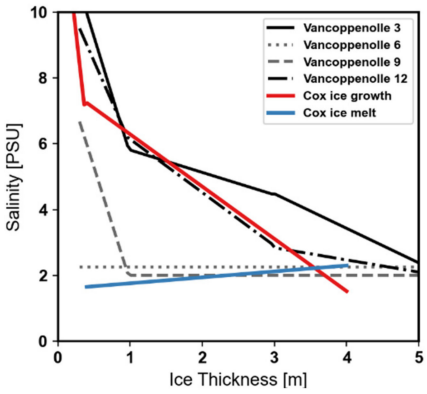

Figure 7. Sea ice bulk salinity formula [44]. The black and gray lines show the bulk salinity curves with ice thickness in different seasons, and the numbers in the legend indicate the month. The red line represents Cox's winter experience formula, and the blue line represents Cox's summer experience formula.

Since the empirical equation of salinity by Vancoppenolle's model takes into account the effects of seasons and is in better agreement with the empirical equation of Cox, in this paper, both were used as salinity for the SMRT single-layer model input.

In addition to the empirical relationship between sea ice bulk salinity and thickness, for the salinity profile equation of the multi-layer model, some studies have considered the uniformity of salinity distribution in sea ice due to gravity drainage and have given the salinity distribution curve in sea ice. For example, both the MYI salinity profile proposed by Schwarzacher et al. (Equation (5), called the Schwarzacher1959) [45] and the FYI and MYI salinity profiles proposed by Griewank et al. (Equation (6), called the Griewank2015) [46] parameterize salinity as a function of normalized sea ice depth. However, there are some differences in the parameterization methods of the two equations. Schwarzer1959 assumes that the salinity of multi-year ice follows a saturation curve where the salinity no longer increases after reaching a certain depth. In contrast, Griewank2015 represents the salinity as an L-shaped curve, with low salinity near the surface and a rapid rise at the bottom.

$$S_i = \frac{1}{2} S_{\max} \left[1 - cos\left(\pi \times z^{0.407/(z+0.573)} \right) \right], \; S_{\max} = 3.2PSU \tag{5}$$

$$\begin{array}{l} S_i = \frac{z}{0.17083} + \left(\frac{z}{0.92762} \right)^{\frac{1}{0.024516}}, \; For\; MYI \\ S_i = \frac{z}{1.0964 - 1.0552 \times z} + 4.41272, \; For\; FYI \end{array} \tag{6}$$

where z is the normalized sea ice thickness, ranging from 0 to 1. $z = 0$ indicates the surface of sea ice, and $z = 1$ indicates the bottom of sea ice. S_i is the sea ice salinity at normalized ice thickness z. In order to further study the accuracy of the Schwarzacher1959 and Griewank2015 salinity profile equations, we compared them with MOSAiC in situ salinity data. The MOSAiC expedition collected ice cores at different depths of sea ice to obtain in situ salinity profiles. The comparison of MOSAiC's salinity profile with the empirical formulas of Schwarzacher1959 and Griewank2015 is shown in Figure 8.

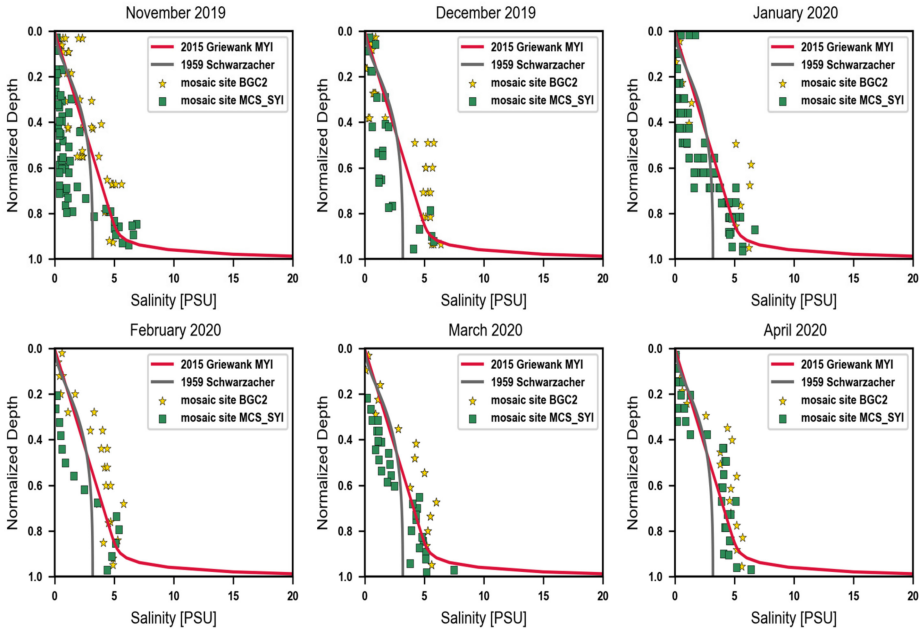

(**a**)

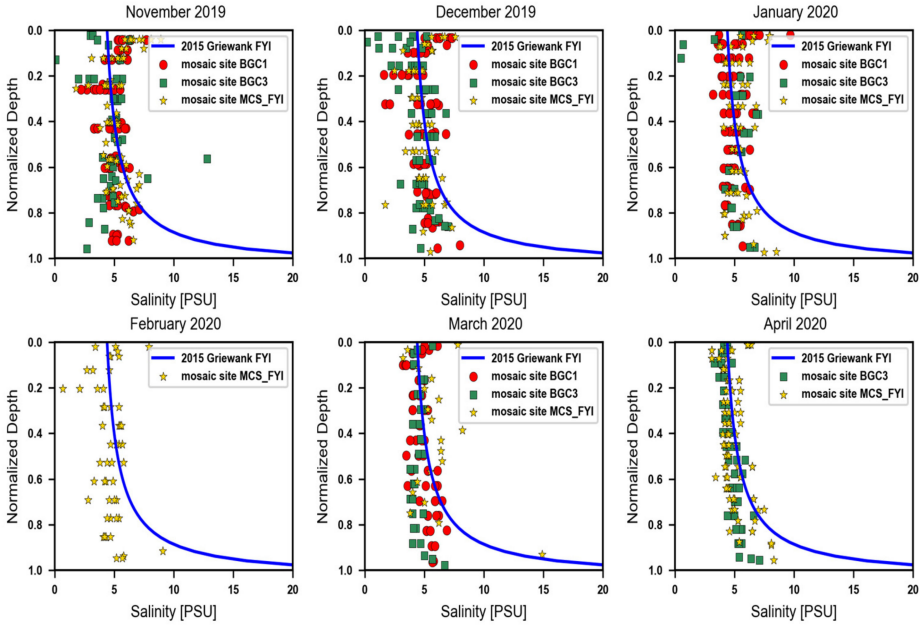

(**b**)

Figure 8. Comparison of MOSAiC in situ data with empirical formulas of Schwarzacher1959 and Griewank2015. (**a**) MYI salinity profile. The salinity data of MOSAiC's BGC2 and MCS_SYI sites were measured on the SYI. (**b**) FYI salinity profile. The salinity data of MOSAiC's BGC1,3 and MCS_FYI sites were all measured on the FYI.

It can be seen that all three have good consistency. Therefore, the salinity profile curves of Schwarzacher1959 and Griewank2015 were adopted in this paper as the salinity input of the SMRT multi-layer model, and the sea ice was set as five layers.

The simulation results of the SMRT model using four salinity formulas are shown in Figure 9. Schwarzacher1959 mainly provided the MYI salinity profile, so only multi-year ice simulation was carried out using this salinity formula.

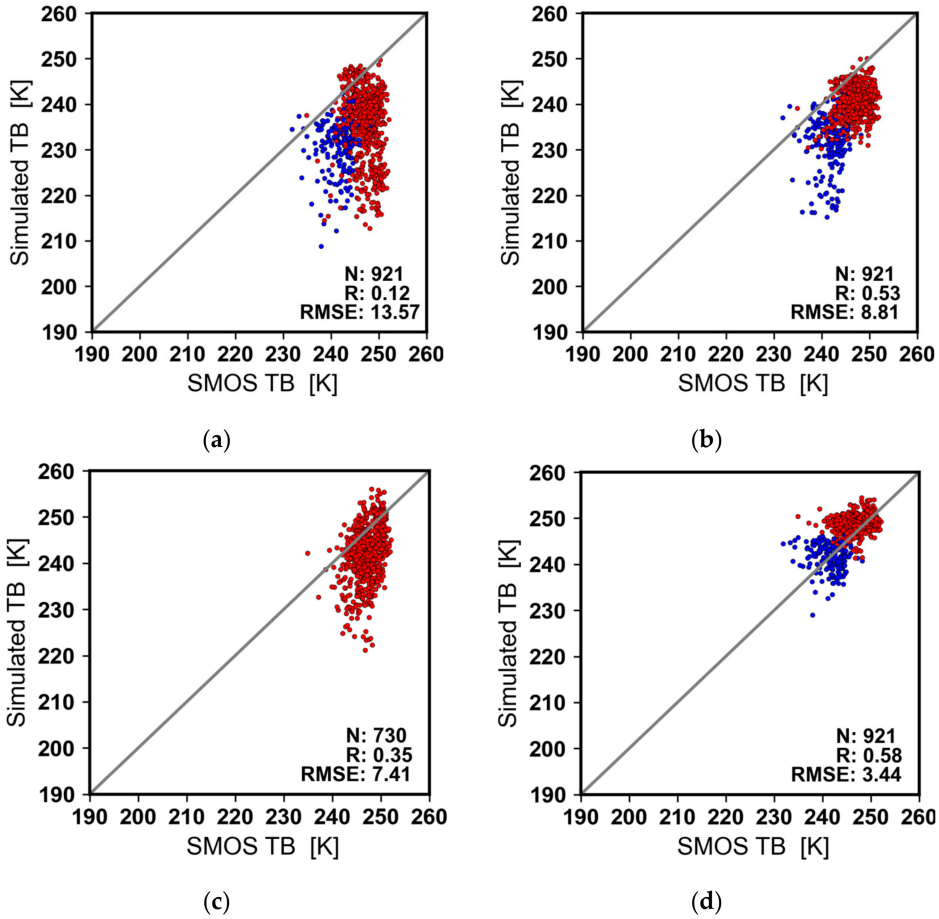

Figure 9. Simulation results of SMRT model in four salinity formulas. The red dots are MYI, and the blue dots are FYI. (**a**) Bulk salinity of Cox. (**b**) Bulk salinity of Vancoppenolle. (**c**) Salinity profile of Schwarzacher1959. (**d**) Salinity profile of Griewank2015. The gray lines are 1:1 lines.

As can be seen from Figure 9, in the L-band Arctic sea ice TB simulation of the SMRT model, only the empirical formula of Griewank2015 in the multi-layer model obtained better simulation results, which may be due to defects in the way of calculating the effective permittivity of sea ice in the SMRT model. Moreover, because of the vertical distribution of temperature and salinity inside the sea ice in practice, the multi-layer model can simulate the actual physical condition of sea ice better than the single-layer model. In the following research, we used the Griewank2015 salinity profile as the input of the SMRT multi-layer model, and the sensitivity of this model to each parameter at this time is shown in Figure 10.

As can be seen from Figure 10, when simulated with the SMRT multi-layer model containing the thermodynamic equation, the salinity empirical formula of Griewank2015, the relationships between simulated L-band TB and the parameters are in good agreement with those reported in previous studies of MYI. For FYI, the multi-layer model achieves similar sensitivity results at lower sea ice salinity to the single-layer model at high salinity.

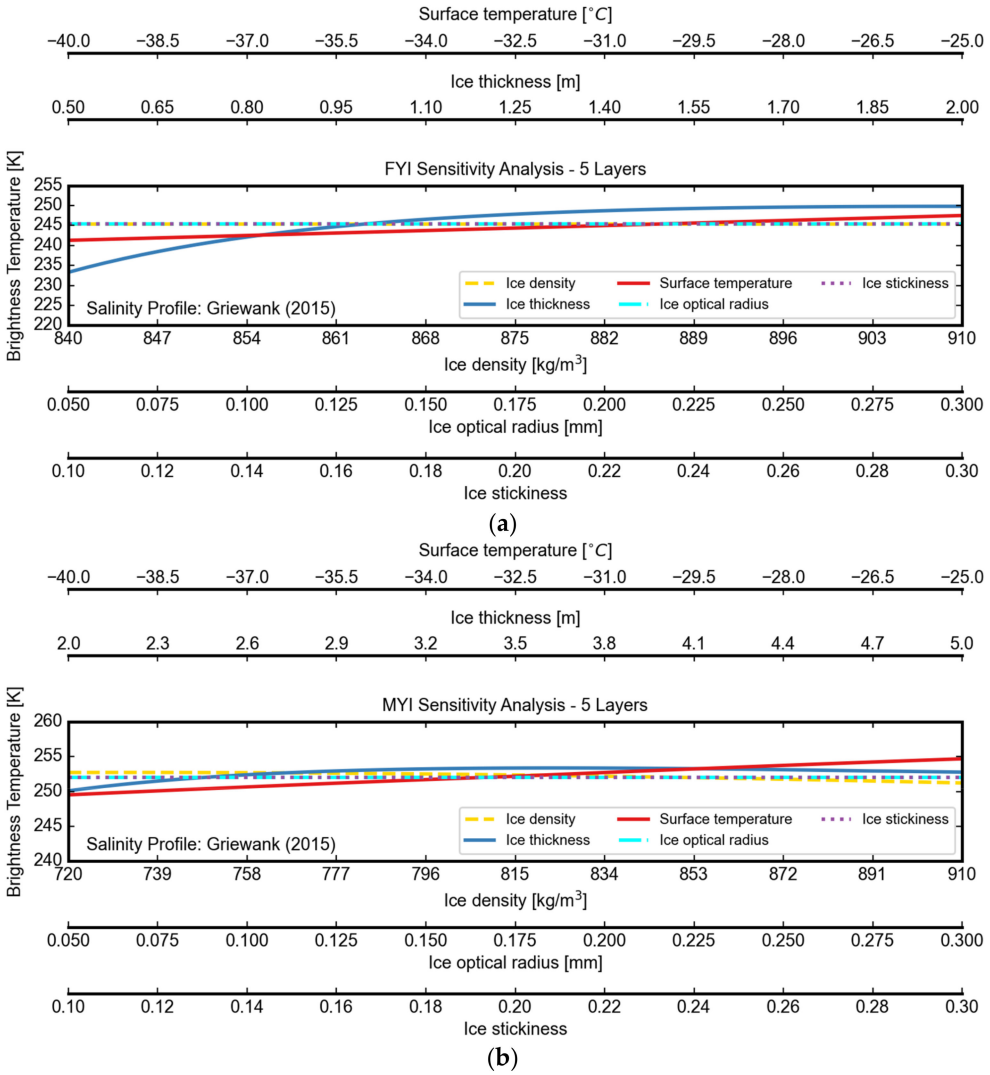

Figure 10. Sensitivity analysis of the SMRT multi-layer model. (**a**) Sensitivity analysis of FYI. (**b**) Sensitivity analysis of MYI.

3.3.3. Sea Ice Leads

Since the actual resolution of SMOS satellite TB data is 40 km, the TB captured by each grid is influenced by the composition of the surface geography. Previous studies proposed that ice leads contained within the ice have a decreasing effect on TB. In order to better evaluate the accuracy of the SMRT model, we also considered the influence of ice leads on the simulated TB.

Figure 11 shows the geographical distribution of simulated TB bias (SMOS TB—simulated TB) and ice leads on 1 and 3 April 2015, with ice lead data from Willmes [34]. It can be seen that in grids with few or no ice leads, the simulated TB bias is small, and when there are more ice leads in the grid, the simulated TB of SMRT is significantly higher than the SMOS TB because the area of ice leads can be water or refrozen thin ice, where the TB is lower than in thick ice. Therefore, the influence of ice leads on simulated TB cannot be ignored.

Figure 12a shows the simulation result of the SMRT model on 22 March 2012, when there were no ice leads, and it is in good agreement with the TB of the SMOS satellite. Figure 12b shows the simulation of the SMRT model on 1 and 3 April 2015. It can be seen that when the ice leads rate is large, the simulation results have obvious bias, and the relationship between this bias and the ice leads rate is shown in Figure 12c. Finally, Figure 12d shows the correlation between simulation bias at all points of the OIB and the ice leads rate from 2012 to 2015. As we can see from the Figure 12c,d, there is a linear

relationship between ice leads and simulation bias, so we used an empirical fit to correct for simulated TB in the ice lead region. The empirical equation for the error correction of ice leads was obtained for the grid with an ice leads rate greater than 0.1, as shown in Formula (7). The dashed black lines in Figure 12c,d represent this empirical equation.

$$Add\_lead\_bias = -18 \times ice\ leads\ rate,\ ice\ leads\ rate \in [0.1, 1] \quad (7)$$

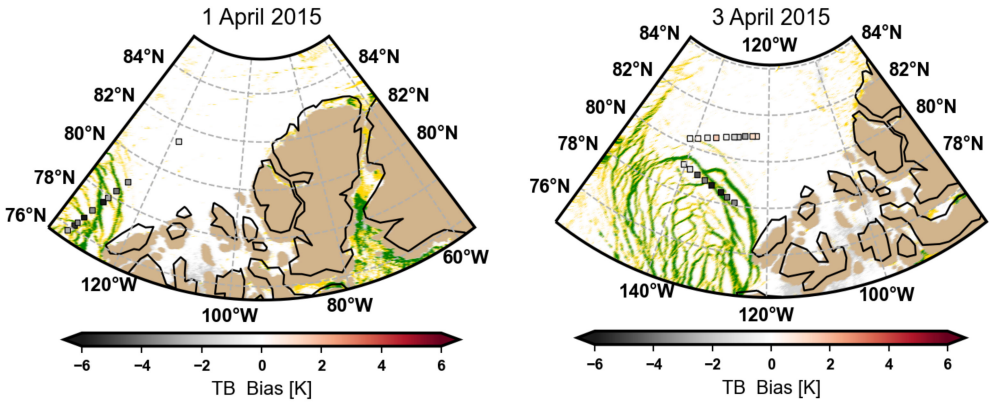

Figure 11. Geographical distribution of simulated TB bias (SMOS TB—simulated TB) and ice leads. The background map shows the distribution of MODIS ice leads, with land in brown, clouds in gray, sea ice in white, ice leads in green, and artifacts in yellow. The color bar shows the value of simulated TB bias.

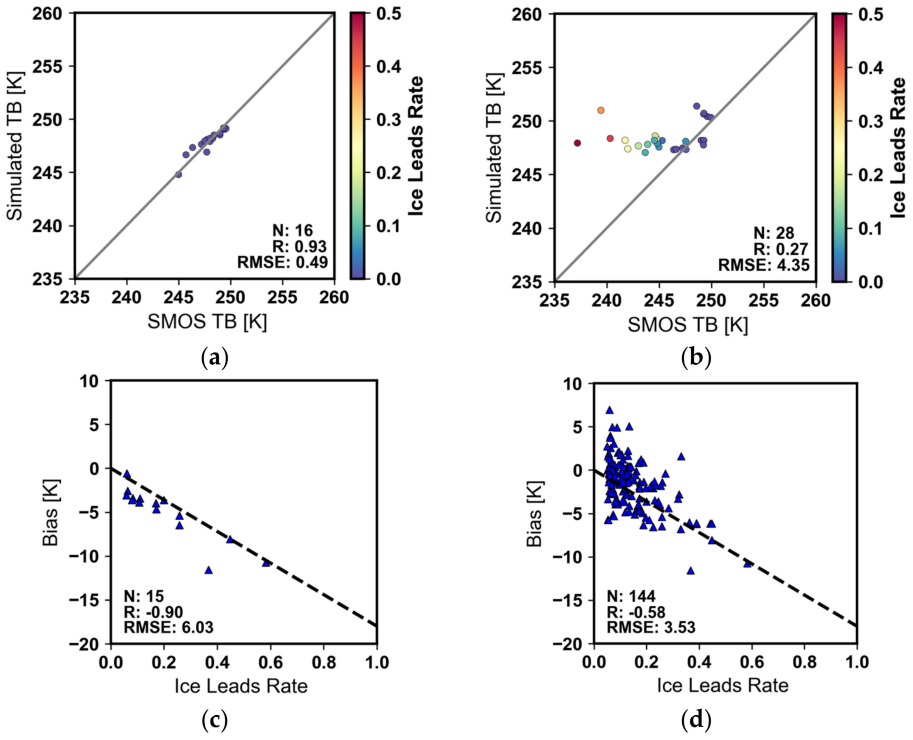

Figure 12. Correlation of simulation TB bias (SMOS TB—simulated TB) and ice leads rate. (**a**) Simulated TB of 22 March 2022, the day without ice leads. (**b**) Simulated TB of 1 April and 3 April 2015, which contained obvious ice leads. (**c**) The correlation between the simulation bias (SMOS TB—simulated TB) and ice leads rate on 1 April and 3 April 2015. (**d**) Correlation between simulation bias at all points of OIB and ice leads rate from 2012 to 2015. The solid gray lines are 1:1 lines. The dashed black lines represent empirical equation between simulation TB bias and ice leads rate.

Through the empirical equation, the simulation results of the SMRT model were corrected. Taking 1 April and 3 April 2015 as an example, as shown in Figure 13, the bias of the grid with ice leads is significantly reduced. Although the influence of the ice lead refreezing state on TB is different, the correction empirical equation cannot completely eliminate the influence of ice leads; however, it can preliminarily eliminate the large-scale error.

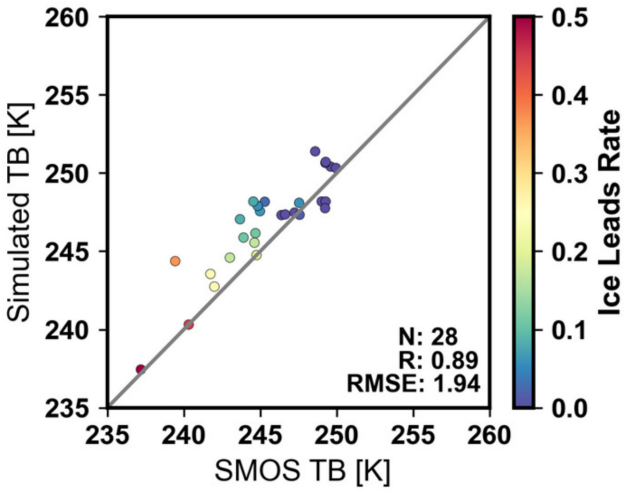

Figure 13. Correlation between simulated TB and SMOS TB after correction for ice leads on 1 April and 3 April 2015. The gray line is the 1:1 line.

4. Results

In this section, the improved simulation method described in Section 3 is used to verify the SMRT model with OIB data and compare it with the KA2010 model. Finally, the SMRT model is applied to the whole Arctic region to test its applicability.

4.1. Evaluation Using OIB In Situ Data

To evaluate whether the improved SMRT model can be used for TB simulations in the Arctic, we compared the simulation results with SMOS observed TB using the OIB in situ data from 2012–2015 as the model input. At the same time, in order to accurately evaluate the model performance, we added the simulation results of the KA2010 model as a comparison. Since Richter et al. [18] compared the KA2010 and M2013 models, and the M2013 model is not used in this paper, only the simulation results of the SMRT and KA2010 models were compared here to illustrate the ability of the SMRT model to simulate the L-band TB in the Arctic ice and snow environment. When using KA2010 for simulation, we selected the empirical formula of bulk salinity [43] contained in the model. Since this empirical formula is only applicable to ice thickness of 0–4 m, and the L-band TB reaches saturation at 4 m, the grid point with ice thickness greater than 4 m was assumed to be 4 m during the simulation.

The simulation results of the two models are shown in Figure 14. It can be seen in Figure 14a,b that the R between the simulation results of the SMRT multi-layer model and the TB of the SMOS satellite is 0.65, and the RMSE is 3.11 K, and the R between the simulation results of the KA2010 model and the TB of the SMOS satellite is 0.51, and the RMSE is 7.25 K. Although the simulation results of KA2010 model are about 6 K lower overall, the two models have a good agreement with SMOS TB. The low result of KA2010 simulation may be due to the fact that it only considers the thermal insulation effect of snow [18].

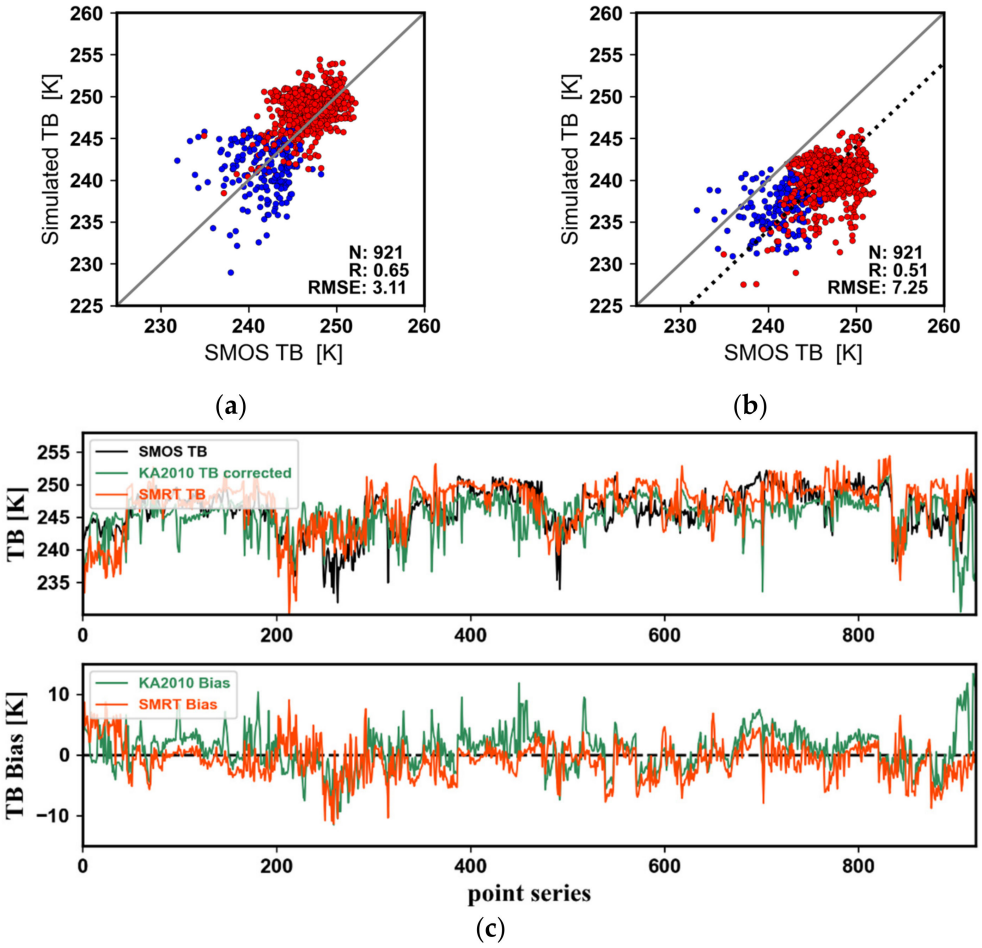

Figure 14. Simulation results of SMRT and KA2010 using OIB in situ data from 2012 to 2015. The red dots are MYI, and the blue dots are FYI. (**a**) SMRT multi-layer model simulation results. (**b**) KA2010 model simulation results. The solid gray lines are 1:1 lines. The dotted black line is the 1:1 line offset by 6k. (**c**) Point sequence diagram of simulation results of SMRT and KA2010 models on the measured OIB data from 2012 to 2015.The dashed black line is the zero bias line.

Figure 14c shows the point sequence of simulation results and bias for the SMRT and KA2010 models; in order to intuitively compare the simulation trend of the two models, we increased the simulation result of KA2010 by 6 K in Figure 14c. It can be seen from the sequence of simulated TB and SMOS satellite TB that the two models simulate the trend of SMOS TB, and the bias of both models is relatively consistent.

The simulation results using OIB in situ data as input parameters show that the SMRT multi-layer model containing the snow and ice thermodynamic equation, the empirical equation of Griewank2015, is able to simulate the general variation of TB in the L-band over Arctic sea ice and snow.

4.2. Arctic-Wide Applications

The validation using OIB in situ data shows that the SMRT model is able to simulate the L-band TB in the Arctic. However, due to the spatial and temporal coverage of OIB in situ data, we needed some satellite data as input when applying the SMRT model to the whole Arctic region.

Due to data limitations, we mainly observed the influence of ice leads on the simulated TB in March and April, and ice leads were most obvious in April during our study period. Figure 15 shows a scatter plot illustrating the differences in simulation bias between SMRT and KA2010 and the ice leads rate in April 2015. The dashed black line in the figure indicates the correction empirical equation obtained from experiments using OIB in situ

data, that is, Formula (7). It can be seen that the scatter points between the simulated bias using satellite data and ice leads fit well with the correction empirical equation of OIB, indicating that Formula (7) can be used to correct the TB bias caused by ice leads. However, due to the different thickness of ice refrozen in ice leads, the TB error is also different, so the correction empirical equation of ice leads can only represent the typical influence.

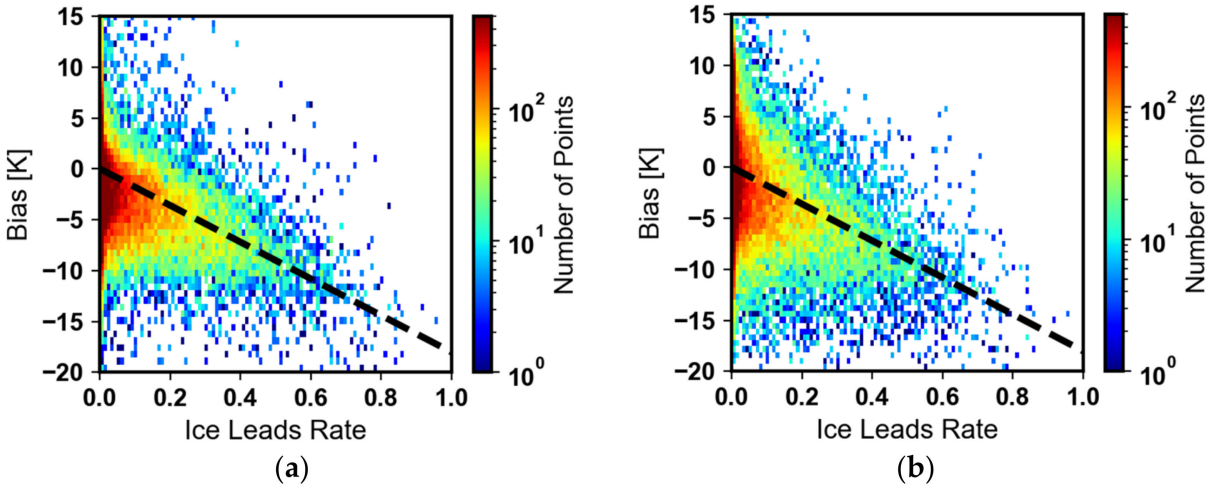

Figure 15. Scatter points between the simulated bias using satellite data and ice leads in April 2015. The black dashed line in the figure is Formula (7). (**a**) Scatter points between the SMRT model simulated bias using satellite data and ice leads. (**b**) Scatter points between the KA2010 model simulated bias using satellite data and ice leads. For an intuitive comparison, this figure also increases the overall simulation result of KA2010 by 6 k.

Figure 16 shows the simulated TB and bias of the SMRT model before and after the correction of ice leads on 5 April 2015, when there was significant ice leads. It can be seen that before the correction, the simulated TB was significantly higher than the satellite TB in the ice lead region, and after the correction, the simulated TB tended to be consistent with the satellite TB. Although there was still some bias, the obvious influence of ice leads was removed.

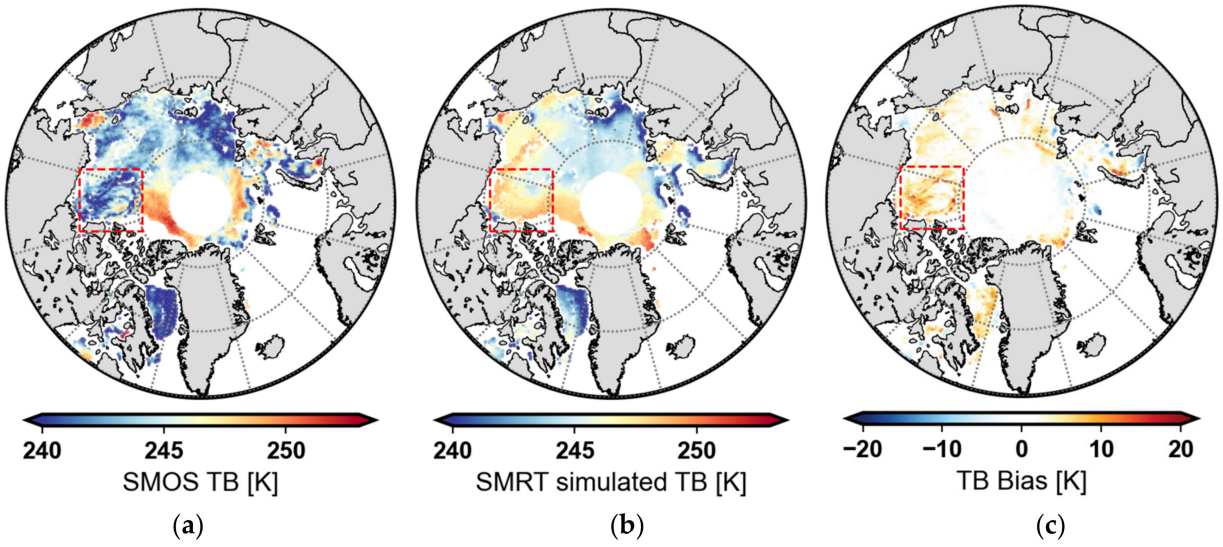

Figure 16. *Cont.*

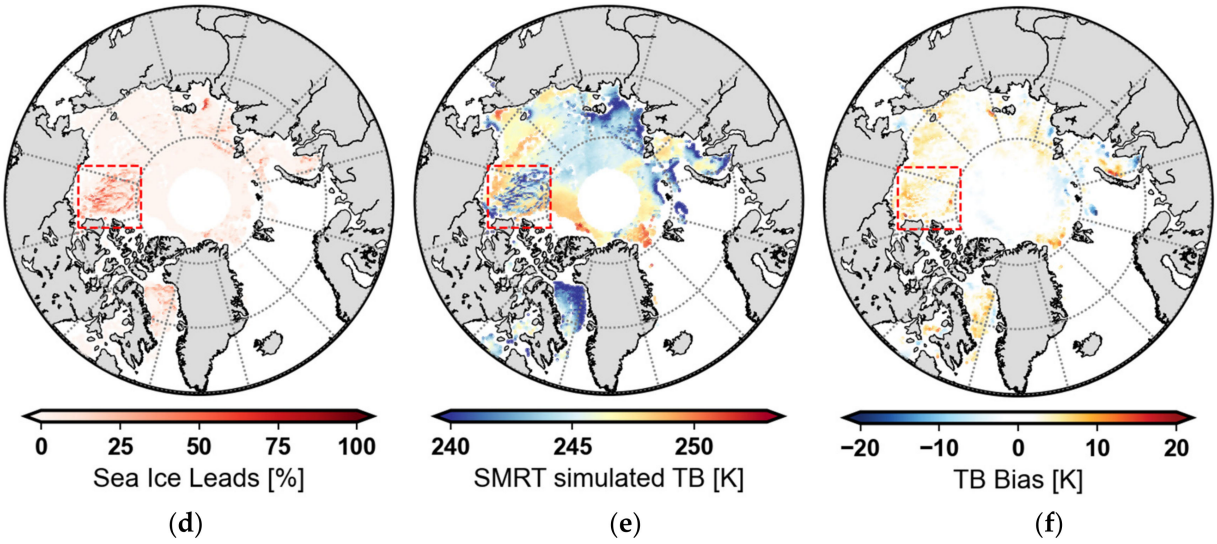

Figure 16. Simulated TB and bias before and after correction of ice leads on 5 April 2015. The red box shows the areas with dense ice leads. (**a**) SMOS satellite TB. (**b**) SMRT simulated TB before correction. (**c**) Simulation bias distribution before correction. (**d**) Distribution of ice leads. (**e**) SMRT simulated TB after correction. (**f**) Simulation bias distribution after correction. The simulation bias was calculated by SMRT TB—SMOS TB.

The simulation results of SMRT and KA2010 were corrected for ice leads, and the results from November 2014 to April 2015 after the correction are shown in Figure 17.

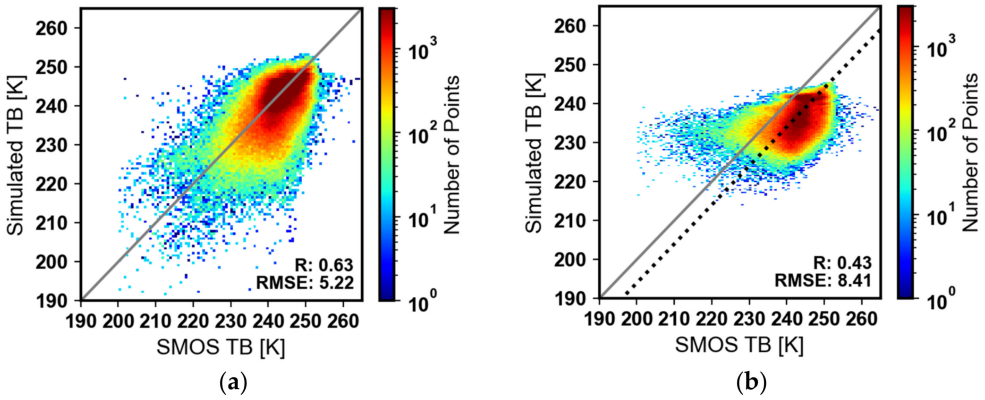

Figure 17. Comparison of SMRT and KA2010 model simulation results with SMOS satellite TB from November 2014 to April 2015. (**a**) SMRT simulation results from November 2014 to April 2015. (**b**) KA2010 simulation results from November 2014 to April 2015. The solid gray lines are 1:1 lines. The dotted black line is the 1:1 line offset by 6k.

As shown in Figure 17, the R between the SMRT-simulated TB and SMOS satellite TB is 0.63, and the RMSE is 5.22 K, and the R between the KA2010-simulated TB and the SMOS satellite TB is 0.43, and the RMSE is 8.41 K. The simulation results of KA2010 are still low, about 6 k, compared to the SMOS TB on the whole. Taking March 2015 as an example, Figure 18 shows the geographical distribution of average monthly SMOS TB and the simulation bias of the SMRT and KA2010 models. The simulation bias of SMRT in the whole Arctic is small compared to KA2010, and although KA2010 simulation results are generally low, both models simulate the general trend of satellite TB.

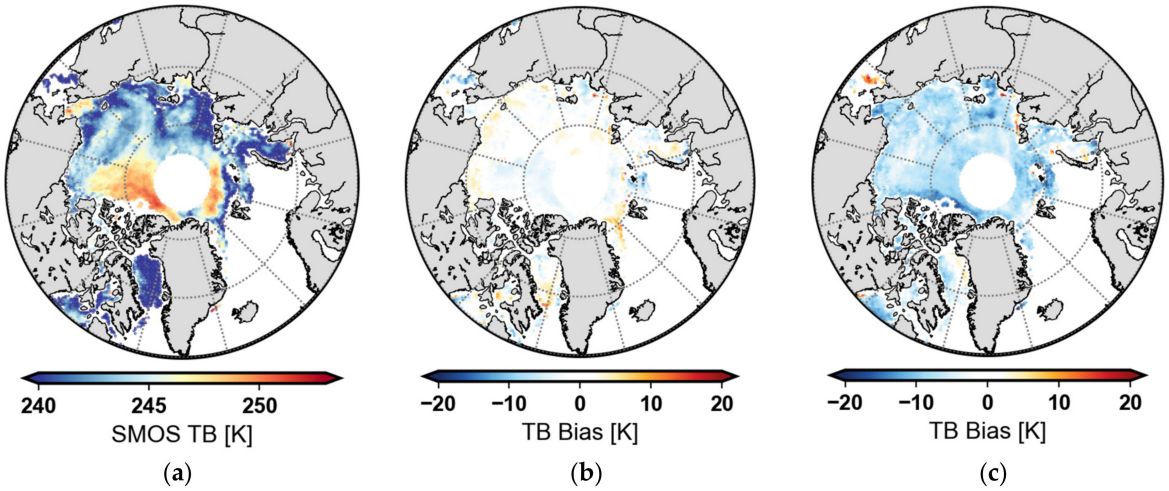

Figure 18. The distribution of the monthly averaged SMOS TB and the simulation bias of SMRT and KA2010 models in March 2015. (**a**) The distribution of SMOS TB. (**b**) The distribution of SMRT TB—SMOS TB. (**c**) The distribution of KA2010 TB—SMOS TB.

5. Discussion

The simulation bias using OIB in situ data as model input is smaller than that using satellite data as input since OIB provides relatively accurate model input data. For simulation using OIB measured data, the bias between model simulation TB and satellite TB may arise for several reasons. First, due to the limitations of the model, it cannot fully physicalize the entire microwave radiative transfer process. Second, the SMOS satellite has instrument accuracy errors, and TB bias occurs in the process of data product processing [35]. Third, the SMRT model is a ground surface radiative transfer model in which the atmospheric part is not fully developed, and the KA2010 model we used does not include atmospheric simulation, so the simulation results in this paper ignore the influence of atmosphere on L-band TB. Finally, there are limitations to the salinity formula and ice lead correction empirical equation. Although the time range of the OIB data is mainly from March to April, the salinity formula and ice lead correction empirical equation cannot accurately represent the sea ice characteristics in all regions. Besides, although OIB provides relatively accurate in situ data, it also has uncertainties which affect the simulation results to some extent. In addition to the above reasons, we did not consider the effect of sea ice concentration, and only took points with sea ice concentration greater than 95% and treated them as 100%, which also caused simulation bias.

There are other sources of bias when using satellite data for simulation than OIB input data. One is the limitation of the model input data. For example, due to the lack of MOD29P1D IST data, although ERA5 SKT can be used as a supplement, the data quality is lower than that of MOD29P1D products. More complete and accurate surface temperature could be used in future research. Moreover, we adopted a unified salinity profile formula for the simulation of the entire Arctic and the entire winter. Although the salinity profile of sea ice with different thickness differs based on the definition of normalized ice thickness, the variability of the salinity formula is not obvious for the entire Arctic and the entire winter, which may also lead to simulation errors.

6. Conclusions

Based on the recently developed snow microwave radiative transfer (SMRT) model, we systematically evaluated its L-band brightness temperature (TB) simulation capability in the Arctic sea ice and snow cover environment. Three improvements were made in the simulation process: first, thermodynamic equations were added to the SMRT model to simulate the thermal insulation effect of snow; second, the influence of single-layer and multi-layer structure and the corresponding salinity formula on the simulation results was

compared; third, the influence of the sea ice leads on the TB was reduced through the fitting formula. The results show that the model can be applied to L-band TB simulation and parameter inversion.

According to the improved simulation method, the SMRT model was evaluated and compared with the snow-corrected KA2010 sea ice model using OIB in situ data. The results show that under reasonable parameter settings, the SMRT multi-layer model can simulate well the L-band TB of the Arctic sea ice and snow environment. The correlation between simulated TB and SMOS satellite TB was 0.65, and the RMSE was 3.11 K; the simulation requirements were met. The simulation results of SMRT were in good agreement with those of KA2010 after 6 k correction. The SMRT model was applied to the whole Arctic using satellite data to simulate TB. The results show that the correlation between SMRT-simulated TB and SMOS satellite TB was 0.63, and the RMSE was 5.22 K from November 2014 to April 2015. This shows that it is feasible to use the SMRT model to simulate L-band TB in the Arctic sea ice and snow environment.

In addition, we used the same model microstructure setup as the DMRT-ML model, which can be applied to L-band microwave radiative transfer simulations, such as the sticky hard spheres microstructure, the DMRT QCA short-range electromagnetic model, and the DORT radiative transfer solution. The SMRT model with an improved simulation method in this framework was successfully applied to the simulation of the whole Arctic. There may be other combinations within the SMRT framework that can be applied to L-band simulations, and this could be a future study. In future work, we will consider combining the SMRT model with atmospheric process simulations to perfect the overall L-band microwave radiative transfer process from ground to satellite. The SMRT model and the improved L-band simulation method will be applied to the retrieval of snow and ice parameters in the future.

Author Contributions: Methodology, Y.F.; Investigation, L.L.; Resources, H.C. and L.G. All authors have read and agreed to the published version of the manuscript.

Funding: This research work was supported by the National Key Research and Development Programs of China (2019YFA0607001) and the National Key Research and Development Project (2021YFC2803300).

Data Availability Statement: The code of SMRT model is available from the website of https://github.com/smrt-model/smrt (accessed on 28 March 2022).

Acknowledgments: We are grateful to the developers of the SMRT model and KA2010 model and thankful to the ESA, NSIDC, ECMWF, and OSI-SAF for providing the research datasets.

Conflicts of Interest: The authors declare no conflict of interest.

References

1. Rees, W.G. *Remote Sensing of Snow and Ice*; CRC Press: Boca Raton, FL, USA, 2006.
2. Waldholz, R. In Western Alaska, There's Water Where There Should Be Ice. Available online: https://www.ktoo.org/2018/02/26/western-alaska-theres-water-ice/ (accessed on 26 July 2023).
3. Pulliainen, J.T.; Grandell, J.; Hallikainen, M.T. HUT snow emission model and its applicability to snow water equivalent retrieval. *IEEE Trans. Geosci. Remote Sens.* **1999**, *37*, 1378–1390. [CrossRef]
4. Wiesmann, A.; Mätzler, C. Microwave emission model of layered snowpacks. *Remote Sens. Environ.* **1999**, *70*, 307–316. [CrossRef]
5. Picard, G.; Brucker, L.; Roy, A.; Dupont, F.; Fily, M.; Royer, A.; Harlow, C. Simulation of the microwave emission of multi-layered snowpacks using the Dense Media Radiative transfer theory: The DMRT-ML model. *Geosci. Model. Dev.* **2013**, *6*, 1061–1078. [CrossRef]
6. Royer, A.; Roy, A.; Montpetit, B.; Saint-Jean-Rondeau, O.; Picard, G.; Brucker, L.; Langlois, A. Comparison of commonly-used microwave radiative transfer models for snow remote sensing. *Remote Sens. Environ.* **2017**, *190*, 247–259. [CrossRef]
7. Wigneron, J.P.; Kerr, Y.; Waldteufel, P.; Saleh, K.; Escorihuela, M.J.; Richaume, P.; Ferrazzoli, P.; de Rosnay, P.; Gurney, R.; Calvet, J.C.; et al. L-band Microwave Emission of the Biosphere (L-MEB) Model: Description and calibration against experimental data sets over crop fields. *Remote Sens. Environ.* **2007**, *107*, 639–655. [CrossRef]
8. Schwank, M.; Rautiainen, K.; Mätzler, C.; Stähli, M.; Lemmetyinen, J.; Pulliainen, J.; Vehviläinen, J.; Kontu, A.; Ikonen, J.; Ménard, C.B.; et al. Model for microwave emission of a snow-covered ground with focus on L band. *Remote Sens. Environ.* **2014**, *154*, 180–191. [CrossRef]

9. Lemmetyinen, J.; Pulliainen, J.; Rees, A.; Kontu, A.; Yubao, Q.; Derksen, C. Multiple-Layer Adaptation of HUT Snow Emission Model: Comparison with Experimental Data. *IEEE Trans. Geosci. Remote Sens.* **2010**, *48*, 2781–2794. [CrossRef]
10. Leduc-Leballeur, M.; Picard, G.; Mialon, A.; Arnaud, L.; Lefebvre, E.; Possenti, P.; Kerr, Y. Modeling L-Band TB at Dome C in Antarctica and Comparison with SMOS Observations. *IEEE Trans. Geosci. Remote Sens.* **2015**, *53*, 4022–4032. [CrossRef]
11. Roy, A.; Leduc-Leballeur, M.; Picard, G.; Royer, A.; Toose, P.; Derksen, C.; Lemmetyinen, J.; Berg, A.; Rowlandson, T.; Schwank, M. Modelling the L-Band Snow-Covered Surface Emission in a Winter Canadian Prairie Environment. *Remote Sens.* **2018**, *10*, 1451. [CrossRef]
12. Maaß, N.; Kaleschke, L.; Tian-Kunze, X.; Drusch, M. Snow thickness retrieval over thick Arctic sea ice using SMOS satellite data. *Cryosphere* **2013**, *7*, 1971–1989. [CrossRef]
13. Burke, W.J.; Schmugge, T.; Paris, J.F.J.J.o.G.R.O. Comparison of 2.8- and 21-cm microwave radiometer observations over soils with emission model calculations. *J. Geophys. Res.* **1979**, *84*, 287–294. [CrossRef]
14. Zhou, L.; Xu, S.; Liu, J.; Lu, H.; Wang, B. Improving L-band radiation model and representation of small-scale variability to simulate TB of sea ice. *Int. J. Remote Sens.* **2017**, *38*, 7070–7084. [CrossRef]
15. Miernecki, M.; Kaleschke, L.; Maaß, N.; Hendricks, S.; Søbjærg, S.S. Effects of decimetre-scale surface roughness on L-band TB of sea ice. *Cryosphere* **2020**, *14*, 461–476. [CrossRef]
16. Maass, N.; Kaleschke, L.; Tian-Kunze, X.; Tonboe, R.T. Snow thickness retrieval from L-band TBs: A model comparison. *Ann. Glaciol.* **2017**, *56*, 9–17. [CrossRef]
17. Tonboe, R.T.; Dybkjær, G.; Høyer, J.L. Simulations of the snow covered sea ice surface temperature and microwave effective temperature. *Tellus A Dyn. Meteorol. Oceanogr.* **2011**, *63*, 1028–1037. [CrossRef]
18. Richter, F.; Drusch, M.; Kaleschke, L.; Maaß, N.; Tian-Kunze, X.; Mecklenburg, S. Arctic sea ice signatures: L-band TB sensitivity comparison using two radiation transfer models. *Cryosphere* **2018**, *12*, 921–933. [CrossRef]
19. Kaleschke, L.; Maaß, N.; Haas, C.; Hendricks, S.; Heygster, G.; Tonboe, R.T. A sea-ice thickness retrieval model for 1.4 GHz radiometry and application to airborne measurements over low salinity sea-ice. *Cryosphere* **2010**, *4*, 583–592. [CrossRef]
20. Picard, G.; Sandells, M.; Löwe, H. SMRT: An active–passive microwave radiative transfer model for snow with multiple microstructure and scattering formulations (v1.0). *Geosci. Model Dev.* **2018**, *11*, 2763–2788. [CrossRef]
21. Vargel, C.; Royer, A.; St-Jean-Rondeau, O.; Picard, G.; Roy, A.; Sasseville, V.; Langlois, A. Arctic and subarctic snow microstructure analysis for microwave TB simulations. *Remote Sens. Environ.* **2020**, *242*, 111754. [CrossRef]
22. Sandells, M.; Picard, G.; Lowe, H.; Maass, N.; Winstrup, M.; Brucker, L.; Leduc-Leballeur, M.; Larue, F.; Aublanc, J.; Thibaut, P.; et al. Community Development of the Snow Microwave Radiative Transfer Model for Passive, Active and Altimetry Observations of the Cryosphere. In Proceedings of the 2021 IEEE International Geoscience and Remote Sensing Symposium IGARSS, Brussels, Belgium, 12–16 July 2021; pp. 852–855.
23. Sandells, M.; Lowe, H.; Picard, G.; Dumont, M.; Essery, R.; Floury, N.; Kontu, A.; Lemmetyinen, J.; Maslanka, W.; Morin, S.; et al. X-Ray Tomography-Based Microstructure Representation in the Snow Microwave Radiative Transfer Model. *IEEE Trans. Geosci. Remote Sens.* **2022**, *60*, 4301115. [CrossRef]
24. Picard, G.; Löwe, H.; Mätzler, C. Brief communication: A continuous formulation of microwave scattering from fresh snow to bubbly ice from first principles. *Cryosphere* **2022**, *16*, 3861–3866. [CrossRef]
25. Picard, G.; Leduc-Leballeur, M.; Banwell, A.F.; Brucker, L.; Macelloni, G. The sensitivity of satellite microwave observations to liquid water in the Antarctic snowpack. *Cryosphere* **2022**, *16*, 5061–5083. [CrossRef]
26. Soriot, C.; Picard, G.; Prigent, C.; Frappart, F.; Domine, F. Year-round sea ice and snow characterization from combined passive and active microwave observations and radiative transfer modeling. *Remote Sens. Environ.* **2022**, *278*, 113061. [CrossRef]
27. Polder, D.; van Santeen, J.H. The effective permeability of mixtures of solids. *Physica* **1946**, *12*, 257–271. [CrossRef]
28. Kaleschke, L.; Tian-Kunze, X.; Maaß, N.; Mäkynen, M.; Drusch, M. Sea ice thickness retrieval from SMOS TBs during the Arctic freeze-up period. *Geophys. Res. Lett.* **2012**, *39*, L05501. [CrossRef]
29. Vant, M.R.; Ramseier, R.O.; Makios, V. The complex-dielectric constant of sea ice at frequencies in the range 0.1–40 GHz. *J. Appl. Phys.* **1978**, *49*, 1264–1280. [CrossRef]
30. Cox, G.F.; Weeks, W.F. Equations for determining the gas and brine volumes in sea-ice samples. *J. Glaciol.* **1983**, *29*, 306–316. [CrossRef]
31. Ricker, R.; Hendricks, S.; Kaleschke, L.; Tian-Kunze, X.; King, J.; Haas, C. A weekly Arctic sea-ice thickness data record from merged CryoSat-2 and SMOS satellite data. *Cryosphere* **2017**, *11*, 1607–1623. [CrossRef]
32. Rostosky, P.; Spreen, G.; Farrell, S.L.; Frost, T.; Heygster, G.; Melsheimer, C. Snow depth retrieval on Arctic sea ice from passive microwave radiometers—Improvements and extensions to multiyear ice using lower frequencies. *J. Geophys. Res. Ocean.* **2018**, *123*, 7120–7138. [CrossRef]
33. Hall, D.K.; Riggs, G.A. *MODIS/Terra Sea Ice Extent and IST Daily L3 Global 4 km EASE-Grid Day, Version 61*; NASA National Snow and Ice Data Center Distributed Active Archive Center: Boulder, CO, USA, 2021. [CrossRef]
34. Willmes, S.; Heinemann, G. Daily pan-Arctic sea-ice lead maps for 2003–2015, with links to maps in NetCDF format. *PANGEA* **2015**. [CrossRef]
35. Tian-Kunze, X.; Kaleschke, L.; Maass, N. *SMOS Daily Polar Gridded Brightness Temperatures*; Digital Media, ICDC, University of Hamburg: Hamburg, Germany, 2012.

36. Muhuri, A.; Gascoin, S.; Menzel, L.; Kostadinov, T.S.; Harpold, A.A.; Sanmiguel-Vallelado, A.; López-Moreno, J.I. Performance Assessment of Optical Satellite-Based Operational Snow Cover Monitoring Algorithms in Forested Landscapes. *IEEE J. Sel. Top. Appl. Earth Obs. Remote Sens.* **2021**, *14*, 7159–7178. [CrossRef]
37. Timco, G.W.; Frederking, R.M.W. A review of ice density. *Cold Reg. Sci. Technol.* **1996**, *24*, 1–6. [CrossRef]
38. Alexandrov, V.; Sandven, S.; Wahlin, J.; Johannessen, O.M. The relationship between sea ice thickness and freeboard in the Arctic. *Cryosphere* **2010**, *4*, 373–380. [CrossRef]
39. Heygster, G.; Hendricks, S.; Kaleschke, L.; Maaß, N.; Mills, P.; Stammer, D.; Tonboe, R.T.; Haas, C. *L-Band Radiometry for Sea-Ice Applications*; Technical Report; University of Bremen: Bremen, Germany, 2009.
40. Batrak, Y.; Müller, M. On the warm bias in atmospheric reanalyses induced by the missing snow over Arctic sea-ice. *Nat. Commun.* **2019**, *10*, 4170. [CrossRef] [PubMed]
41. Yu, Y.; Rothrock, D.A. Thin ice thickness from satellite thermal imagery. *J. Geophys. Res.* **1996**, *101*, 25753–25766. [CrossRef]
42. Untersteiner, N. Calculations of temperature regime and heat budget of sea ice in the central Arctic. *J. Geophys. Res.* **1964**, *69*, 4755–4766. [CrossRef]
43. Cox, G.F.N.; Weeks, W.F. Salinity Variations in Sea Ice. *J. Glaciol.* **2017**, *13*, 109–120. [CrossRef]
44. Vancoppenolle, M.; Fichefet, T.; Goosse, H. Simulating the mass balance and salinity of Arctic and Antarctic sea ice. 2. Importance of sea ice salinity variations. *Ocean Model.* **2009**, *27*, 54–69. [CrossRef]
45. Schwarzacher, W. Pack-ice studies in the Arctic Ocean. *J. Geophys. Res.* **1959**, *64*, 2357–2367. [CrossRef]
46. Griewank, P.J.; Notz, D. A 1-D modelling study of Arctic sea-ice salinity. *Cryosphere* **2015**, *9*, 305–329. [CrossRef]